ANALISYS OF TRANSVERSE CRACKING IN UNIDIRECTIONAL COMPOSITE PLIES BY MEANS OF COMPUTATIONAL MICROMECHANICS

D. F. Mora[a*], C. Gonzalez[a,b], C. S. lopes[a] , F. Naya[a], J. Llorca[a,b]

[a]*IMDEA Material Institute, Calle Eric Kandel 2, Getafe (Madrid), 28906*
[b]*Department of Materials Science, Polytechnic University of Madrid and CISDEM, UPM-CSIC ETS de Ingenieros de Caminos, 28040 Madrid, Spain*
**diego.mora@imdea.org*

Keywords: transverse cracking, composite failure, FEA

Abstract

The primary aim in this study is to capture the in-situ failure mechanisms in the transverse direction in a $\lfloor 0_2/90_{n/2} \rfloor_s$ *E-glass/Epoxy laminate. A representative volume element (RVE) of the composite microstructure is simulated by using a finite element analysis to capture the main damage mechanism including matrix cracking, fiber-matrix interface debonding and crack propagation of transverse cracks and the consequence crack density. Finally, the relation between the thermomechanical properties and the crack density is studied. The numerical results from the model confirm the insitu strength effect due to the reduction of the thickness of the ply oriented at 90º.*

1. Introduction

Fiber-reinforced polymers (FRP) are nowadays extensively used in applications where outstanding mechanical properties are necessary in combination with significant weight reductions. FRP present several different physical failure mechanisms and the dominant ones depend on the loading conditions. Fracture due to tensile stresses parallel to the fibers is controlled by the tensile fracture of the fibers, while compressive stresses along the fibers lead to fracture by fiber kinking in compression. Tensile fracture perpendicular to the fibers is brittle and is controlled by the fracture of the polymer matrix and of the fiber-matrix interface, while fracture caused by compressive stresses perpendicular to the fibers or by shear is accompanied by large deformations as a result of the non-linear response of the matrix when subjected to compression and/or shear. Finally, as composite laminates are made up by stacking lamina (or plies) with different fiber orientation, interply delamination is another typical failure mechanism in FRP due to the thermo-elastic mismatch between adjacent plies. Despite all existing information and current knowledge about these materials, the accurate prediction of the failure stress of composite materials and structures has been an elusive problem because of the complexity of failure micromechanisms involved.

2. Computational simulation of transverse cracking

Simulations were performed with the Abaqus/Standard finite element package under generalized plain strain conditions in the framework of finite deformations using the initial unstressed state as the reference.

2.1. Geometrical model and finite element discretization

The representative volume element (RVE) used in the analysis corresponds to a cross-ply $\left[0_2/90_{n/2}\right]_s$ laminate (n=1,2,4,8) subjected to tensile loads along the 0º direction (Figure 1.a). The RVE was rectangular in shape with length L=10mm and thickness $t=2(n/2+2)t_0$ being t_0=68.75μm the thickness of a single lamina. The RVE was long enough to adequately capture the cracking pattern and accurately compute the crack density for a given applied deformation. The external laminae with the fibers along the 0º direction were assumed to be homogeneous while the central region of thickness t_0 was discretized with a dispersion of monosized circular E-glass fibers of radius R=15 μm embedded in the polymer matrix.

The fibers were dispersed using the random sequential adsorption algorithm developed by Segurado and LLorca [1], for a given volume fraction of reinforcement. The dispersion of fibers was enforced to maintain the periodicity condition along the loading axis, hence the fibers intersecting the loading edges at x=0 and x=L were cut and translated to the opposite edge of the model. The fiber distribution was generated randomly and sequentially. Each of the fiber position was accepted according to practical requirements to avoid distortions during finite element discretization. It should be mentioned that those fibers intersecting the internal edges at $z=\pm nt_0$ were removed from the model to represent the typical rich matrix region between adjacent plies with different angle directions (Figure 3.b). The model has a fiber volume fraction of 65%.

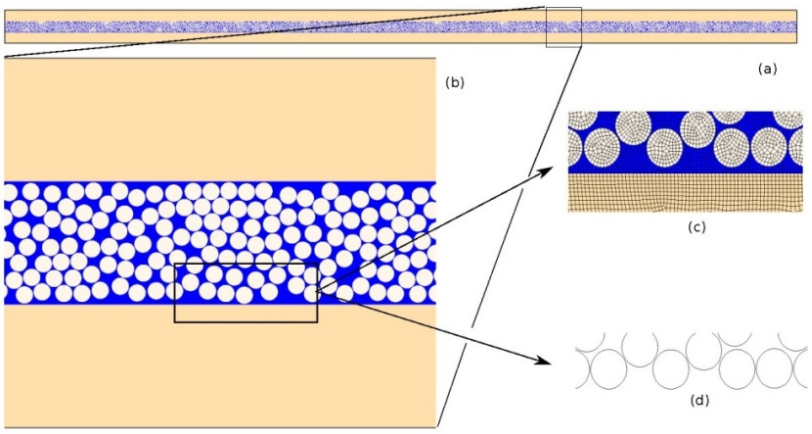

Figure 1. a) RVE of material composite laminate with stacking sequence $[0_2,90_{n/2}]_s$, b) RVE with t=137.5μm and 250 fibers, c) Fiber and matrix mesh detail, d) cohesive elements detail (COH2D4).

2.2 Boundary conditions

Periodic boundary conditions were applied to the edges of the RVE to maintain the continuity between adjacent RVE's which should deform as jigsaw puzzles. The periodic boundary conditions can be expressed by constraint relations between the displacement vector $\vec{u}(x,z)$ of those nodes belonging to the opposite edges. Mathematically, this condition is given by

$$\begin{aligned} \vec{u}(0,z) - \vec{\delta}_x &= \vec{u}(L,z) \\ \vec{u}(x,-t/2) - \vec{\delta}_z &= \vec{u}(x,t/2) \end{aligned} \tag{1}$$

wherein $\vec{\delta}_x = (\delta_x, 0)$ stands for the imposed displacement vector in the loading direction and $\vec{\delta}_z = (0, \delta_x)$ is computed from the condition that the average stresses in the through-the-thickness direction should be zero, the plane stress condition in the x-y plane of the laminate is given by $\int_0^L \vec{t}\, dx = \vec{0} \quad along \quad z = t/2$.

The strain applied to the laminate was computed from the imposed displacement δ_x along the x-direction and was given by $\varepsilon = \delta_x / L$. The average stress acting on the loading edges N_x was computed with the conjugate to the applied displacement reaction force and the current cross section of the laminate. Residual stresses develop in the composites upon cooling at ambient temperature after curing was taken into account in the micromechanical model by simulating the composite behavior in two steps. In the first step, the RVE was subjected to a homogeneous temperature change of $\Delta T = 100^{o} C$ from the stress-free temperature down to ambient temperature (curing to room temperature drop).

2.3 Mechanical behavior of the constituent materials

The material behavior used in this study was previously reported by Canal et al [2,3] and corresponds to an E-glass/MTM 57 epoxy resin manufactured by Advanced Composites Group (ACG). The properties of the fibers, matrix and fibre/matrix interfaces were determined experimentally and were used as inputs in previous computational micromechanical models subjected to uniaxial compressive stress states [2], as well as in simulations of fracture induced by the presence of a notch [3]. During tensile splitting, fiber/matrix decohesion took place prior the severe plastic deformation of the matrix ligaments between neighboring fibers. This initial cracking mechanism was followed by subsequent ductile tearing of the matrix material. The simulation scheme was able to capture adequately the deformation and damage mechanisms observed at the microscale and also the global stress-strain response.

2.3.1. Matrix properties

In this work, the tension-compression directional behavior of the matrix was simulated by means of the damage-plasticity model proposed by Lee and Fenves [5] based on a previous model developed by Lubliner [6]. In this model, two different damage variables are used to account for matrix damage in tension and compression, D_t^m and D_c^m respectively. The model follows the traditional assumption of additive decomposition of the elastic and plastic strains tensors as $\varepsilon = \varepsilon^e + \varepsilon^{pl}$. The stress-strain relation is

$$\sigma = (1 - D^m) C : (\varepsilon - \varepsilon^{pl}) = (1 - D^m) \bar{\sigma} \tag{2}$$

wherein σ is the current stress tensor, D^m is the matrix damage variable (depending on the tensile and compressive damage variables) and C is the initial or undamaged elastic isotropic stiffness tensor that is computed with the respective matrix elastic modulus and Poisson ratio of $E_m = 3.5 GPa$ and $\nu_m = 0.35$. The thermal expansion coefficient of the matrix was set to $\alpha_m = 20x10^{-6} K^{-1}$. $\bar{\sigma}$ stands for the effective stress which is computed assuming undamaged matrix $(D^m = 0)$. The evolution of the damage variable D^m is governed by a set of two hardening variables (equivalent plastic strains for the tensile and compressive modes, namely $\tilde{\varepsilon}^{pl} = [\tilde{\varepsilon}_t^{pl}, \tilde{\varepsilon}_c^{pl}]$) and the effective stress tensor $\bar{\sigma}$. The yield function of the model,

$F\left(\bar{\sigma},\tilde{\varepsilon}^{pl}\right)\leq 0$, accounts for the different evolution of the matrix behavior under tension and compression by means of the expression

$$F\left(\bar{\sigma},\tilde{\varepsilon}^{pl}\right)=\frac{1}{1-\alpha}\left[\alpha I_1+\sqrt{3J_2}+\beta\left(\tilde{\varepsilon}^{pl}\right)\left\langle\hat{\sigma}_{\max}\right\rangle\right]-\bar{\sigma}_c\left(\varepsilon^{pl}\right)\leq 0 \tag{3}$$

wherein $\langle\cdot\rangle$ denotes the Macaulay brackets, I_1 and J_2 stands respectively for the first total and second deviatoric invariants of the effective stress tensor and $\hat{\sigma}_{\max}$ is the maximum principal effective stress (first eigenvalue of the effective stress tensor). The function $\tilde{\varepsilon}^{pl}$ depends on the tensile and compressive strength of the matrix, as follows

$$\beta\left(\varepsilon^{pl}\right)=\frac{\bar{\sigma}_c\left(\varepsilon^{pl}\right)}{\bar{\sigma}_t\left(\varepsilon^{pl}\right)}(1-\alpha)-(1+\alpha) \tag{4}$$

wherein α is the pressure sensitivity parameter determined as $\alpha=\sigma_{b0}-\sigma_{c0}/2\sigma_{b0}-\sigma_{c0}$ with σ_{b0} and σ_{c0} being the biaxial and uniaxial compressive strength of the matrix. Finally, the matrix tensile and compressive damage variables are assumed to be determined by the plastic equivalent strains in tension and compression $D_t^m=D_t^m\left(\varepsilon_t^{pl}\right)$ and $D_c^m=D_c^m\left(\tilde{\varepsilon}_c^{pl}\right)$ and the degraded response of the matrix material obtained from the equivalent matrix damage variable as $D^m=1-\left(1-D_t^m\right)\left(1-D_c^m\right)$.

In tension, damage occurs when the matrix stress reaches the tensile strength $\sigma_t^m=75MPa$ and the softening region is governed by a matrix fracture energy of $G_f^m=100\,J/m^2$. On the other hand, damage is suppressed in the compressive region, and plastic yielding without hardening occurs at a compressive strength of $\sigma_c^m=105MPa$.

2.3.2. Fiber/matrix interface properties

Fiber/matrix interface decohesion was simulated using the cohesive crack model. Isoparametric four-noded cohesive elements (COH2D4 in Abaqus/Standard) with thickness $10^{-3}\mu m$ were inserted at the fibers/matrix interfaces. The mechanical behavior of the interface can be expressed in terms of a traction-separation law. In the absence of damage, the interface elements behave linearly and elastically with an initial stiffness given by K_i. The traction vector in this case is

$$t_n=K_i\delta_n \quad and \quad t_s=K_i\delta_s \tag{5}$$

wherein t_n and t_t, are the normal and tangential components of the traction vector and δ_n and δ_t, the respective conjugate displacement jumps at the interface. The elastic stiffness of the interface was set to $K_i=5x10^7\,MPa/\mu m$ to ensure continuity of the displacement and stress fields in the absence of damage. The onset of damage occurs when the traction vector acting on the interface reaches the interface strength and this is dictated by the interactive quadratic stress criterion which reads as

$$\left(\frac{\langle t_n \rangle}{N}\right)^2 + \left(\frac{t_t}{S}\right)^2 = 1 \tag{6}$$

with N and S the normal and shear strength of the interface. After the onset of damage, the stress transmitted by the cohesive crack is reduced according to the damage parameter D^i which evolves from zero in the absence of damage to one at which point the physical interaction across the crack disappears and the crack propagates. In such regime, the normal and tangential components of the traction vector acting on the interface are determined as

$$\begin{aligned} t_n &= (1 - D^i) K^i \delta_n \text{ and } t_n = K^i \delta_n \text{ if } \delta_n \le 0 \\ t_t &= (1 - D^i) K^i \delta_t \end{aligned} \tag{7}$$

The evolution of the damage variable D^i is controlled by the norm displacement jump across the interface $\bar{\delta} = \sqrt{\langle \delta_n \rangle^2 + \delta_t^2}$ according to $d = \bar{\delta}^f \left(\bar{\delta}^{\max} - \bar{\delta}^0\right) / \bar{\delta}^{\max} \left(\bar{\delta}^f - \bar{\delta}^0\right)$.

where $\bar{\delta}^0$ and $\bar{\delta}^f$ stand, respectively for the displacement norm at the onset ($D^i = 0$) and propagation ($D^i = 1$) of cracking. The symbol $\bar{\delta}^{\max}$ is the maximum displacement norm attained during the loading history at the integration point of the element. Crack propagation occurs when the energy release rate equals the interface fracture toughness G_c (area under the traction-displacement cohesive curve). The properties were set to $N = 50MPa$, $S = 75MPa$ and $G_c = 100\, J/m^2$ as in [2].

2.3.3. Fiber and 0º layer properties

E-glass fibers were treated as isotropic thermo-elastic solids in the whole deformation range with Young's modulus $E_f = 74GPa$, Poisson ratio $\nu_f = 0.2$ and thermal expansion coefficient $\alpha_f = 5x10^{-6} K^{-1}$. On the other hand, the constitutive behavior of the layers with the fibers aligned with the loading axis direction was homogenized using the Mori-Tanaka method from the thermo-mechanical properties of the fibers and matrix considering a reinforcement volume fraction of 65%. The lamina elastic constants obtained are $E_1 = 45.7GPa$, $E_2 = 14.5GPa$, $\nu_{12} = 0.26$ and $G_{12} = 4.3GPa$ and the thermal expansion coefficients $\alpha_1 = 6.22e-6$ and $\alpha_2 = 28.9e-6$.

3. Simulation results

Different models were generated using the Python-to-Abaqus scripting, leading to homogeneous fiber distributions corresponding to cross-ply laminates with increasing relative thickness between 90º and the 0º supporting layers. The stacking sequence is in figure 2(a). Models with a maximum element number of three million of elements were run in a AMD cluster with 24 processor leading to maximum computing times of the order of 48 hours.

3.1. Strain to first microcrack

The defined RVE was subjected to two consecutive steps: an initial temperature drop of $\Delta T = 100^o C$ and the mechanical axial in-plane straining. The first stages of the simulation

progressed in an elastic manner. Stress and strain distribution in the fibers and matrix are clearly non-homogeneous and the fiber-fiber variations are controlled by the spatial distribution of the fibers in the RVE. Initially, during the application of the temperature drop, residual stresses in tension develop in the matrix being the magnitude not enough to cause any damage during the cooling down process. This residual stress distribution modifies the onset for matrix cracking formation in the subsequent steps. It is interesting to note that the source of residual stresses at the micro scale is a combination of stresses generated due to the thermoelastic mismatch between fiber and matrix as well as the effects of the different ply orientations in the laminate.

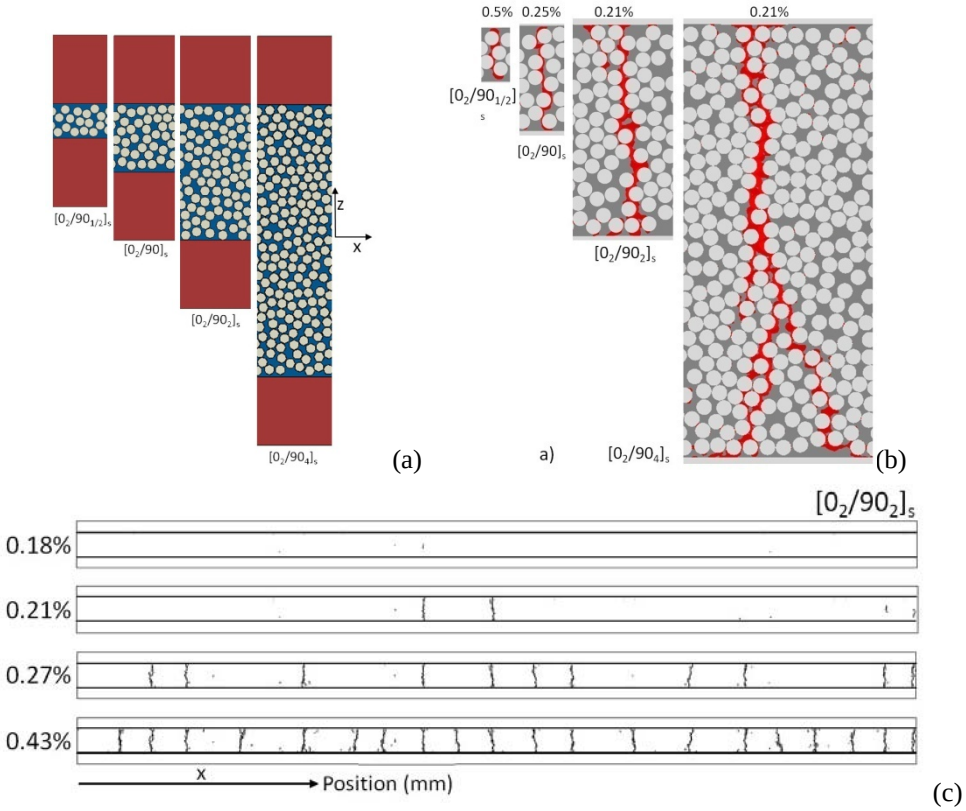

Figure 2. (a) Sections of the RVE of $[0_2,90_{n/2}]_s$ laminates used in the simulation, (b) Snap-shots of the fist ply cracks occurring in the $[0_2,90_{n/2}]_s$ laminate, (c) Cracking pattern evolution with the applied macroscopic strain in the $[0_2,90_2]_s$ laminate.

During the following stages of the thermo-elastic loading, damage occurs at the fiber matrix interface producing decohesion at the fiber poles of some fibers with respect to the x loading axis of the RVE. It should be mentioned that these interface cracks are naturally generated with the present approach and are directly triggered by the internal stresses at the fiber/matrix scale (maximum values) being the corresponding peaks controlled by the spatial distribution of the fibers within the RVE. At some point of the deformation process, damage localization occurs in a section of the laminate linking neighboring fiber/matrix failures and generating voids (equivalent to a continuum crack opening displacement COD) by the interface separation. A quasi-continuous crack is then developed by the coalescence of the interfacial voids and the subsequent plastic deformation and failure of the matrix ligaments between voids, (Figure 2(b) and (c)). After the localization, other interface cracks are closed as a result of the stress release around the formed crack. The tortuosity of the meandering crack path is strongly controlled by the local spatial distribution of the fibers within the RVE.

3.2. Multiple cracking

The mechanical performance of the laminate is not strongly affected by the occurrence of the first microcrack. However, upon continue loading, the generation of new microcracks produce significant degradation of the in-plane thermomechanical properties of the composite laminate. The in-plane secant elastic modulus in the loading direction, E_x, as well as the in-plane Poisson ratio, ν_{xy} evolve as a function of applied strain and the lay-up configuration. Under these conditions, the homogenized elastic constants for the cracked laminate are determined as:

$$E_x = \frac{\sigma_x}{\varepsilon_x} \; and \; \nu_{xy} = -\frac{\varepsilon_y}{\varepsilon_x} \tag{8}$$

where σ_x is the homogenized laminate stress for a given applied strain ε_x, while ε_y is the out of xz plane deformation obtained from the generalized plane strain condition used in the simulations. The results of the normalized in-plane elastic modulus are presented in Figure 3(a) and Poisson ratio in Figure 3(b). They show reduction of the both parameters in all RVEs as the applied strain increases due to the microcracking taking place in the 90º plies. The thicker the 90º layer, the more noticeable is the degradation of the thermomechanical properties.

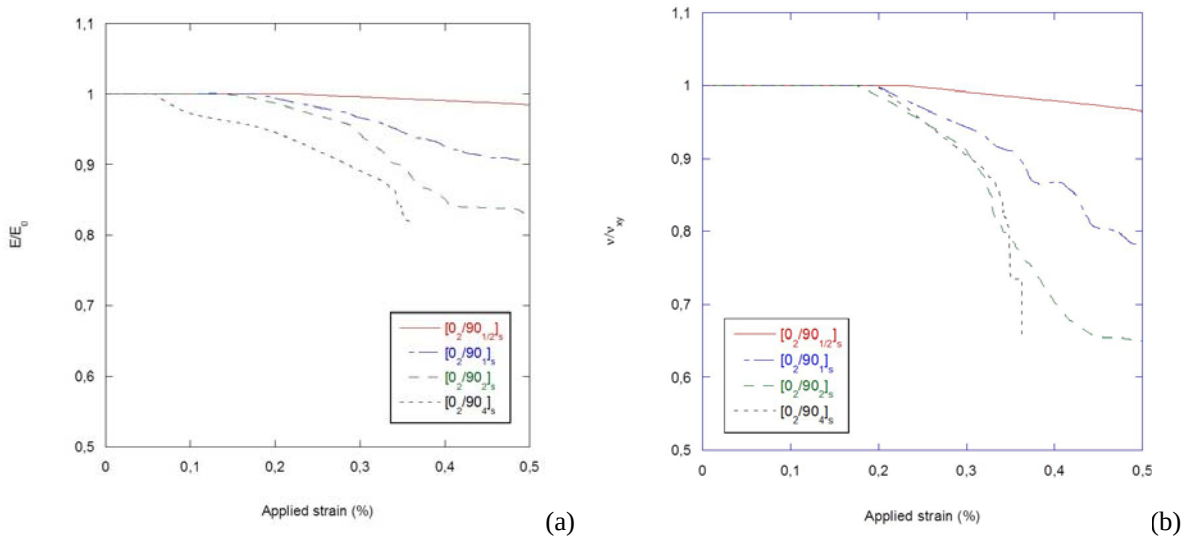

Figure 3. (a) Normalized in-plane elastic modulus, (b) and Poisson ratio evolution with the applied strain for the laminates $[0_2,90_{n/2}]_s$.

4. Conclusions

A computational micromechanics model was developed to analyze the matrix crack formation and evolution in fiber reinforced cross ply laminates following a $[0º,90º_{n/2}]_s$ stacking sequence being n=1/2, 1, 2 and 4. According to this modelling strategy, the supporting layers following the loading direction at 0º were modelled as homogenized solids with the corresponding elastic properties of the unidirectional composite lamina while the cracking layers at 90º were modelled using an specific computational micromechanics model with a detailed discretization of the actual composite microstructure. Fibers were distributed in the cracking

layers homogeneously and the solid formed by fibers, matrix and interfaces discretized with finite elements. Damage formation was allowed by the introduction of specific constitutive equations for fibres, matrix and interfaces. Matrix plasticity and damage as well as fiber/matrix debonding were introduced in the model with detailed constitutive equations which were the deformation and damage mechanisms responsible of the appearance of laminate matrix cracks.

The mechanisms of crack formation were obtained and analyzed in detail and they contrast fairly well with the experimental trends observed in the literature. The macroscopic cracks, were generated by the coalescence of several fiber debondings which concentrated matrix damage in the remaining ligaments. The macroscopic crack progressed towards the supporting layers interface being the tortuosity of the crack more pronounced when dealing with thicker laminates. In this case, the crack branches prior to the arrival to the lamina interface. The subsequent matrix cracking is consistently captured by the model and follows the typical mechanisms reported with shear lag model. After the occurrence of matrix crack, the stress in the area is relaxed increasing the probability of matrix cracking in adjacent layers beyond the zone controlled by the shear lag recovery.

References

[1] J. Segurado, J. LLorca. A numerical approximation to the elastic properties of sphere-reinforced composites, Journal of the Mechanics and Physics of Solids 50 (10):2107-2121, 2002

[2] L. Canal, C. Gonzalez, J. Molina-Aldaregua, J. Segurado, J. LLorca. Application of digital image correlation at the microscale in fiber-reinforced composites, Composites Part A (10), 1630-1638, 2012.

[3] L. Canal, G. Gonzalez, J. Segurado, J. LLorca. Interply fracture of fiber reinforced: microscopic mechanisms and modeling, Composite science and technology 72 (11), 1223-1232. 2012.

[4] J. Lubliner,J. Oliver, S. Oller, E. Oñate, A plastic-damage model for concrete, International Journal of Solids Structures 25 (3). 299-326. 1989.

[5] J. Lee, G. Fenves, Plastic-damage model for cyclic loading of concrete structures, Journal of Engineering Mechanics 124 (8) 892-900. 1998.